Reduction to monostatic focusing of bistatic or motion uncompensated SAR surveys

A. Monti Guarnieri, F. Rocca
Dipartimento di Elettronica - Politecnico di Milano
Piazza Leonardo da Vinci 32 - 20133 Milano Italy
FAX +39 02 23993413 - TEL +39 02 2399 3446
E-mail:monti@elet.polimi.it

Abstract

We study the response due to a point scatterer in a rather general case of bistatic surveys. We derive the relative time - space function, that we call Flat Top Hyperbola. The complexity of this curve motivates the reduction of a general bistatic survey to a monostatic one, following the techniques used in seismic data processing. The scatterers correspondent to a single received pulse in a bistatic configuration are located on the intersection of the ground plane with an isochronal ellipsoid that has source and receiver as foci. These scatterers are then considered as targets of a monostatic configuration. Thus, we reduce a bistatic configuration to a monostatic one, by identifying an approximate space varying transfer function between the two configurations. This paper, sequel to other recently published, addresses also the problem of motion compensation, in that the first survey could also be monostatic, and the location of the second monostatic survey is at choice. The use of a Digital Elevation Model is shown to be essential for the correct determination of the transfer function in the general case. It is not necessary if source and receivers have a constant distance and follow the same trajectory.

Introduction

In these last years there has been an impressive growth in the interest in bistatic radar [1]. In the field of Synthetic Aperture Radar, constellations of multiple spaceborne sensors like the Cartwheel should be available in the next future [2], [3], while first bistatic airborne SAR acquisitions have been completed with success [4], [5], [6]. As a consequence, a growing literature is appearing on bistatic focusing. Depending on the geometry, the bistatic configuration, the antenna aperture and the bandwidth, the processing of such systems can be as simple as a tuning of a monostatic processor, or a real challenge [7]. Several papers approach the "stationary" case, with parallel orbits and same velocity, either by exploiting proper approximations, like small antenna apertures [8], [9], or by exact solutions [10], [11].

Other

papers approach the more general case of different orbits and velocities, apart from the exact, but computational expensive backprojection technique in [12], this case is still taken again to a monostatic approach by a proper, approximated pre-processing [7], [13]. Despite this rich literature, the development of an efficient phase preserving focusing scheme is still a challenging issue due to the requirement for massive data processing on one side and the design of wide-aperture, wide-bandwidth SAR on the other.

This paper, read in part at the 2004 EUSAR Meeting,

comes after

paper [11], where introductory remarks on the technique of transforming bistatic into monostatic surveys are discussed. We will refer to [11], [14], and [15] for a proper understanding of the geophysical approach, the terminology, and the general modeling. With respect to [11] where the constant offset case between source and receiver was discussed, there is here a significant innovation in that the 3D character that is peculiar to more general bistatic SAR surveys is taken into account.

We remind that the technique that we shall discuss here is usual in geophysics, where up to 6000 (six thousand!) receivers can operate simultaneously, and where normally the surveys have a full 3D character. We refer to the recent work by Fomel [15] for a complete and thorough discussion of the approximations implicit in this approach. The approximation is weaker for non uniform media where the velocity changes are significant in the volume shared by the two acquisitions. This situation is in general far from those encountered with

SAR, unless localized atmospheric or ionospheric artifacts change significantly the velocity of the rays of one survey with respect to the other.

The motivation of this work is to establish a general framework to categorize the bistatic surveys transforming them into a monostatic one.

Bistatic surveys may use opportunity transmitters, and thus the surveying geometry might be rather unusual. Therefore, it is useful to find a general tool (space variant, indeed) that applies to all bistatic geometries, naturally space variant, transforming them into the space invariant monostatic geometry, indicating the instances where the transformation proposed in [11] could not be applied. Sure enough, in many cases, extreme squints, and unlikely geometries can be avoided. However, there will also be cases where the opportunity source and the position of the receiver will be such that this work could be of interest. Thus we decided not to enter into the discussion of synthetic cases, that would anyway be biased towards a specific geometry, not necessarily the one of interest in the case to be studied.

We begin with a short discussion of the problem of focusing, in the case of rather general bistatic surveys, and we provide the travel time curve (called the Flat Top Hyperbola FTH) that gives, for a preassigned position of a point scatterer located on the ground plane, the total travel time from source to the scatterer and then back to the receiver as a function of the positions of the source and receiver. Then, focusing can be carried out as usual by combining (say with a weighted sum) the received data at the times correspondent to the FTH so that we can estimate the reflectivity of the scatterer. This technique could be computationally expensive. Furthermore, it does not characterize fully the inherent differences between a bistatic and a monostatic configuration.

Successively, we introduce a different approach to focusing: we identify first an ellipse on the ground plane, intersection of it with the isochronal ellipsoid that has as foci source and receiver. One single received pulse in the bistatic survey is what we would have seen if we had scatterers nowhere else but along that ellipse. The illumination function provided by the directivity of the transmitter and of the receiver obviously would limit this ellipse to a small part.

Then, we can suppose to carry out a monostatic survey onto this elliptical distribution of scatterers; further, we evaluate the outcome of such a survey.

So, we will be able to carry out a transformation from any received pulse in a general bistatic configuration into a travel time curve (the generalized smile) in a monostatic one, i.e. we will identify the transfer function between the two configurations. The peculiarities of the generalized smile are useful to appreciate the impact of the bistatic configuration. Finally, we will deal with the case of motion compensation, where both configurations are monostatic but different. Short conclusions will follow.

1 The bistatic geometry

Before discussing the general geometry of a bistatic survey, let us first appreciate its differences with the monostatic case. In a monostatic situation with straight orbit, the acquisition has rotational symmetry - the axis being the orbit itself, - and the survey may be considered 2D, rather than 3D. This compaction from a 3D space to a 2D one cannot happen, for curved orbits, or in a general bistatic survey where source and receiver follow different paths. Thus, the non stationarity of the 3D geometry along azimuth has to be characterized, necessarily complexifying any focusing technique.

Let us consider a general bistatic geometry as in Fig. 1, where the target P is imaged by the bistatic system composed of the sensors S_1 and S_2:

- v_1 and v_2 are the velocity of the two sensors on their trajectory, assumed rectilinear,

- r_{z1} and r_{z2} are the closest approach distances of the target with respect to the two sensors

- τ_{z1} and τ_{z2} are the azimuth times at which each sensor is in the closest approach with respect to the target

We can assume S_1 to be transmitting and S_2 receiving, and define τ as the azimuth, slow-time. The sensors - target - distances at any time τ are then:

$$r_1(\tau; P) = \sqrt{(\tau - \tau_{z1})^2 v_1^2 + r_{z1}^2} \tag{1}$$

$$r_2(\tau; P) = \sqrt{\tau^2 v_2^2 + r_{z2}^2}, \tag{2}$$

where we assumed, without loss of generality, that the origin for τ axis is such that $\tau_{z2} = 0$. The bistatic range is obtained by adding (1) and (2):

$$r_b = \sqrt{(\tau - \tau_{z1})^2 v_1^2 + r_{z1}^2} + \sqrt{\tau^2 v_2^2 + r_{z2}^2} \tag{3}$$

$$\phi_b = \frac{2\pi}{\lambda} r_b. \tag{4}$$

The expression (3), usually defined as "Double Square Root" (DSR) summation, describes the bistatic curve known as "Flat Top Hyperbola" (FTH). The bistatic Doppler Phase History, $\phi_b(P)$ in (4), is proportional to the bistatic delay, and depends upon 5 parameters $(v_1, r_{z1}, \tau_{z1}, v_2, r_{z2})$. Eventually we rearrange the DPH

as follows:

$$\phi_b = \frac{2\pi v_1}{\lambda}\left(\sqrt{(\tau-\tau_{z1})^2+\frac{r_{z1}^2}{v_1^2}}+\sqrt{\tau^2\frac{v_2^2}{v_1^2}+\frac{r_{z2}^2}{v_1^2}}\right)$$
$$= \frac{2\pi v_1}{\lambda}\left(\sqrt{(\tau-\tau_{z1})^2+\tau_1^2}+\sqrt{\mu\tau^2+\tau_2^2}\right), \quad (5)$$

where we have introduced the three normalized parameters:

$$\tau_1 = \frac{r_{z1}}{v_1};\ \tau_2 = \frac{r_{z2}}{v_1};\ \mu = \frac{v_2^2}{v_1^2}.$$

We notice that the general shapes of both the DPH and FTH depend upon four parameters $\{\tau_1, \tau_2, \mu, \tau_{z1}\}$, and a scale factor. In the constant offset case [11], $\mu = 1$ and we have three parameters; whereas only one parameter is needed in the monostatic case, where $\tau_1 = \tau_2$; $\mu = 1$; $\tau_{z1} = 0$.

2 Small Aperture

Although the non-stationary, bistatic DPH (5) is quite more complicated than a monostatic one, we can still approximate it by quadratic expansion, at least for very small azimuth apertures, to get a simplified focusing. Let us start from the DPH in (5), and evaluate first the instantaneous frequency:

$$f_\tau = \frac{1}{2\pi}\frac{\partial\phi_b}{\partial\tau} = \frac{v_1}{\lambda}\left(\frac{\tau-\tau_{z1}}{\sqrt{(\tau-\tau_{z1})^2+\tau_1^2}}+\frac{\mu\tau}{\sqrt{\mu\tau^2+\tau_2^2}}\right), \quad (6)$$

and then the second derivative, the fm-rate:

$$k = f'_\tau = \frac{v_1}{\lambda}\left(\frac{\tau_1^2}{\sqrt{\left((\tau-\tau_{z1})^2+\tau_1^2\right)^3}}+\frac{\mu\tau_2^2}{\sqrt{(\mu\tau^2+\tau_2^2)^3}}\right). \quad (7)$$

We finally assume the fm-rate to be constant, $k(\tau_0)$, where τ_0 is the time when the target is at the center of the antenna beam, to allow azimuth focusing by means of any monostatic technique, like the Range Doppler. The non-stationary behaviour could then be handled by tuning the fm-rate with azimuth in block-like fashion (provided that its variation is smooth).

The limit of this technique depends both on the time span of the observed DPH, and the actual slope of its second derivative, i.e. $k'(\tau_0)$. In order to appreciate visually this second aspect, we have drawn in Fig. 2 the DPH and its derivative in an extreme case of a system that is both strongly bistatic and strongly non-stationary. We used (5) by assuming: $\tau_{z1} = 0.4$, $\tau_1 = 0.34$, $\tau_2 = 0.7 \cdot \tau_1$, $\mu = 2$. The figure draws in dash and dotted lines the two Monostatic Hyperbolas (MH), corresponding to the two square roots in (5), together with the resulting DPH, in continuous line, whereas its first derivative, $\phi'_b(\tau)$, is plotted below. We wish that $\phi'_b(\tau)$ approximates that of a monostatic system, therefore we need it to be nearly linear, and this assumption appears reasonable only when τ is far from the vertices of the two MH, where we have fast changes of slope. When τ approaches either τ_{z1} (= 0 in our case) or τ_{z2}, the monostatic-based focusing fails, unless the bandwidth is reduced to a very small value. In that case, as well as in the case of wide bandwidth, we need to develop a different methodology, and this motivates this paper.

We remark that the example has been exaggerated just to provide a visual understanding of the problem: the vertices of the two MH have been made quite sharp by using small values of τ_1, τ_2. In practical spaceborne or airborne systems, these values are two orders of magnitude larger than those used. Notwithstanding, the impact of a non-stationary Doppler rate on the focused impulse response could still be appreciable, particularly for high resolution SARs. In a general case, we expect that the vertex of the DPH is somewhat between the vertices of the two MH (just in the middle for the constant offset), its location has been derived in close form in the appendix and can be used, together with (7), to appreciate the validity of the monostatic approach in the worst case.

3 Reduction of general bistatic to monostatic surveys

In the previous section we have seen a simple approach to focus bistatic surveys. However, the shape of the FTH is close to singular in several cases. It is interesting, at least for comprehension, to transform a bistatic survey into a monostatic one in order to characterize their real differences. On one side, the monostatic survey is azimuth invariant; oppositely, the bistatic surveys can well be azimuth varying. We need an azimuth varying tool that transforms the bistatic surveys into monostatic ones to characterize this change. The approach that we will follow is simple and discussed systematically in the paper [11]. If the input (bistatic) data set is made just by a single pulse, this implies that we have scatterers on the ground plane only on the intersection between the ground plane and the isochronal ellipsoid that has foci at the positions that the source and the receiver had when the pulse was emitted. Then, we revisit this ground distribution of

scatterers with a monostatic survey. The result of this survey, namely a distribution of arrivals in time and space, will correspond to the space varying 2D transfer function between the bistatic and the monostatic survey. Its characteristics will elucidate the non stationarity of the bistatic survey and will allow us to understand the changes with respect to a monostatic one. The same analysis goes for the case of motion compensation: the data are acquired from a trajectory and transferred to another. This will allow us to discuss the case when the synthetic aperture is wide with respect to the variation of the fm-rate, and the DPH cannot be approximated with a second order curve as previously suggested. In this case, we shall see that, given the DEM, it is possible to derive a generalized smile [11]. Another point that should be considered is that with this way of operation, it will be easy to accommodate for the antenna pointing at the receiver and transmitter ends to evaluate any amplitude effects. Furthermore, in the case of a strong scatterer, its correct amplitude will be recovered combining together all the arrivals; however, we refer to [15] for studies on the correct distribution of amplitudes and illumination.

3.1 The need of a Digital Elevation Model

Before entering simple geometrical analyses, we would like to show how it comes that focusing bistatic surveys may be dependent on the information about the location of the scatterers in the 3D space. This effect is clarified in the example shown in Fig.3. Two different bistatic configurations are there shown: in case (a) the two sensors move along the same track, with a proper displacement. In case (b), they follow two parallel tracks. Two targets P_a and P_b, are drawn; they are seen at the same (bistatic) time when the midpoint between source and receiver is at azimuth $\tau = 0$, since they belong to the same isochronal ellipsoid with these foci. In the case (a) of aligned tracks, the two targets (and any target on a circle C centered on the track) will have the same (delay, Doppler) coordinates in the data space, hence the same FTH would result for both targets. In this case the data would span a 2D space, like for monostatic SAR, and a DEM characterizing the position of the targets on the circle C would be useless. On the opposite, in the case (b) when the axis of the ellipsoid is no longer aligned with the sensor track, the third dimension becomes relevant, as each target along the circle C generates a different FTH in the (t, τ) domain. Then, the 3D spatial imbedding is important and a DEM would be required to reconstruct both the shape and the position of each FTH, in order to perform a proper focusing. An incorrect Digital Elevation Model would lead to defocusing (in that, using an incorrect FTH, we would neglect to pick up and combine some of the available Doppler components and we would pick up and combine some components containing only noise).

These considerations may appear finicky, but with an increasingly wider relative bandwidth of the SAR data, like the unprecedented PAMIR SAR [16], the quality of the focusing has to be greater and greater, reaching the limit when the relative bandwidth approaches 2.

3.2 Focusing using the pull technique

We will provide here an example of focusing a bistatic survey, with no constraints at all on the antenna aperture, under the following assumptions: (1) targets lay on the flat ground; (2) orbits are straight and parallel to the ground (but not necessarily parallel to each other), and coplanar (same altitudes for both tracks). We assume that sensors may have different velocities. Although the case is pretty general, it is not the most general we can conceive. However, we shall see in the next section that the procedure proposed here is flexible and can be extended to all the other cases.

Let us assume the geometry sketched in Fig. 4. The figure shows the two sensors, S_1 and S_2, their track, and the track of their mid-point. We assume a reference system with the x-axis oriented like the mid-point along-track (azimuth), $O(\tau)$, the z-axis perpendicular with respect to ground (here assumed flat) and the $x-$axis perpendicular to the yz plane, as usual.

Let us apply the linear superposition to the input data (in the data space), and let us suppose that we have a single spike, at azimuth, range time ($\tau = 0, t = t_b$). This spike corresponds to a distribution of scatterers located on an ellipsoid that has foci in the position of the sensors at the acquisition time ($\tau = 0$). Notice that the axis of symmetry of the ellipsoid is, in general, not parallel to the x-axis. We assume that locally it slants at an angle ψ, shown in the figure. The equation of the ellipsoid can be written in the local reference (x', y', z) that is rotated of ψ with respect to the reference (x, y, z) (the x' axis is shown in the figure as well):

$$\frac{x'^2}{a_e^2} + \frac{y'^2}{b_e^2} + \frac{z^2}{b_e^2} = 1 \tag{8}$$

$$a_e = \frac{ct_b}{2}$$

$$h = \sqrt{a_e^2 - b_e^2} \Rightarrow b_e = \sqrt{\left(\frac{ct_b}{2}\right)^2 - h^2}.$$

The sensor location at $\tau = 0$, that corresponds to the

foci is written in the same reference as

$$S_1\left\{x'=h, y'=0, z=h_s\right\};\ S_2\left\{x'=-h, y'=0, z=h_s\right\}$$

We suppose that the scatterers lie on the ground plane. Therefore, for each spike in the data space, a uniform distribution results in the model space of scatterers along an ellipse as shown in the figure:

$$\frac{x^{'2}}{a_e^2}+\frac{y'^2}{b_e^2}=1-\frac{h_s^2}{b_e^2} \tag{9}$$

$$\frac{x'^2}{a^2}+\frac{y'^2}{b^2}=1$$

$$a=a_e\sqrt{1-\frac{h_s^2}{b_e^2}}$$

$$b=b_e\sqrt{1-\frac{h_s^2}{b_e^2}}=\sqrt{b_e^2-h_s^2}, \tag{10}$$

which corresponds to an impulse in the data. The focusing is then carried out by means of the "pull" technique, summing along each flat top hyperbola correspondent to each point of the ground plane. To check the correctness of this approach, we can now model back the scatterer along an ellipse in the data space by means of a tomographic approach. For each of the scatterers in the model space, that compose the ellipse, we backproject (spread, push) a FTH in the data-space. The sum of all these FTH reproduce the spiky data set, as shown in Fig. 5.

3.3 Generalized smile

The way we convert a generalized bistatic system into a monostatic one plus a proper pre-processing step follows closely the derivation in [11].

The geometry now is much different, in that the targets are located on a plane in a 3D space (the flat earth spanned by azimuth, and ground range) and no more in the azimuth, slant range reference. This situation is far from the constant-offset case (coincident orbits, equal velocity).

As said in [11], we map the distribution of scatterers onto a monostatic survey, correspondent to a spike in the initial bistatic survey. Then, focusing will correspond first to the convolution of the initial data with the *generalized smile*, i.e. the ellipse in the ground plane back as seen from the monostatic trajectory of choice, to be followed by the usual monostatic focusing. In a following section we will also show how even motion compensation can be seen under this perspective, leading to an intrinsic identification of motion compensation and bistatic focusing.

As the ground plane imprint of any monostatic SAR is a circle, we decompose the elliptically-shaped reflector on the ground as a superposition of many circular-shaped reflectors, each of them tangent to the ellipse: the idea is explained in Fig. 6 .

The geometry is detailed in Fig. 7: the target P on the ground belongs both to the ellipsoid coming from bistatic survey and to the circle coming form the monostatic survey with center in M. We represent the ellipse (9), intersection of the initial ellipsoid (8) with the ground plane of the scatterers, with an envelope (superposition) of circles. We have to impose a common tangent between the ellipse and the generic circle. For each target on the ellipse $P(x'=a\cos\phi, y'=b\sin\phi, z=0)$, the tangent angle is

$$\frac{dy'}{dx'}=-\frac{b\cos\phi}{a\sin\phi},$$

and the equation of the normal to the tangent in P (the line P-C in Fig. 7.b) is then:

$$\eta-b\sin\phi=\frac{a\sin\phi}{b\cos\phi}\left(\xi-a\cos\phi\right)$$

$$a\xi\sin\phi \quad -\left(a^2-b^2\right)\sin\phi\cos\phi= \ b\eta\cos\phi,$$

the center of the circle, C is the intersection with the line $\eta=\xi\tan\psi$. The coordinates of C are thus:

$$C(x'=\xi_0, y'=\xi_0\tan\psi, z=0) \tag{11}$$

$$\xi_0=\frac{\left(a^2-b^2\right)\sin\phi\cos\phi}{a\sin\phi-b\cos\phi\tan\psi}.$$

The monostatic delay is proportional to the radius of the sphere centered in M (see Fig. 7.a):

$$M(x'=\xi_0, y'=\xi_0\tan\psi, z=h_s),$$

and passing through P:

$$P(x'=a\cos\phi, y'=b\sin\phi, z=0).$$

The delay is thus:

$$t_m=\frac{2}{c}\left|P-M\right| \tag{12}$$

$$\frac{t_m^2c^2}{4}=\left(a\cos\phi-\xi_0\right)^2+\left(b\sin\phi-\xi_0\tan\psi\right)^2+h_s^2,$$

and thus we get a distribution of spikes to be added to the monostatic survey in positions located along the x-axis with abscissa equal to the distance $|C-O'|$:

$$x=\xi_0/\cos\psi\Rightarrow\xi_0=x\cos\psi. \tag{13}$$

We can finally write the expression of the generalized smile in the azimuth, time domain (in the data-space):

$$\frac{t_m^2c^2}{4}=\left(a\cos\phi-x\cos\psi\right)^2+\left(b\sin\phi-x\sin\psi\right)^2+h_s^2 \tag{14}$$

where the dummy variable ϕ should be removed by exploiting (11) and (13):

$$\xi_0 = \frac{\left(a^2 - b^2\right)\sin\phi\cos\phi}{a\sin\phi - b\cos\phi\tan\psi} = x\cos\psi \qquad (15)$$

and the parameters describing the ellipse, a, b, should be derived from the acquisition geometry, namely the sensors distance, h (slow time variable, now) and the bistatic time, t_b, according to (8) and (9):

$$b_e = \sqrt{\left(\frac{ct_b}{2}\right)^2 - h^2} \qquad (16)$$

$$a = \frac{ct_b}{2}\sqrt{1 - \frac{h_s^2}{b_e^2}}$$

$$b = \sqrt{b_e^2 - h_s^2}, \qquad (17)$$

As an example, Fig. 8.a plots different smiles corresponding to different values of the rotation, ψ. Notice that the parameters of the generalized smile require information about the DEM.

3.4 Discussion; constant offset

It is interesting to look at these generalized smiles to try to identify their message. It is evident that if the antenna pattern is such that only a small part of the ellipse in the ground plane is illuminated, these complex shapes may simplify to the usual chunks of hyperbolas and thus simple second order approximations of the FTH (the usual smiles, then, maybe slightly tilted) could do in most of the cases. However, we also see that in some situations, namely correspondent to the cusps of the generalized smile, the second order expansion would fail and we have to move to more complex descriptions. In some cases, that is, the bistatic configuration does not lead to a simple representation as a monostatic one. We notice that these cusps exist also in the case of constant offset, namely in the usual smile as discussed in the paper [11]. However, in that case, the cusps correspond to energy backscattered from points that are approximately along the survey line, i.e. with extreme squint, and therefore not illuminated with the usual antennas radiation patterns. The possibility of opportunity bistatic surveys, where the geometry is totally random, may make these observations useful.

Another point that we just mention here has also been well discussed in geophysics [17]. This is the azimuth resolution enhancement, made possible by combining multiple bistatic surveys. In fact, combining different transfer functions, one could increase resolution as with multiple sampling, thus gaining the equivalent advantage of an increased PRF. This result has been independently rediscovered in the SAR community, pointing out the advantages of a split receiver antenna for the reduction of the azimuth ambiguities [3], [18].

Finally, a point that should be better analyzed, is the impact of the precision of the DEM on focusing. From the equation 15, within a well defined geometry, some conclusions might be drawn, that however are much too geometry and resolution dependent to be discussed here where we only would like to establish a general framework.

For better clarity, let us now verify that the smile derived in [11] is a particular case of the *generalized smile* here derived, for the constant offset case. We have parallel tracks, hence $\psi = 0$, and (15) can be easily inverted:

$$x = \frac{\left(a^2 - b^2\right)\cos\phi}{a} \qquad (18)$$

$$\cos\phi = \frac{ax}{a^2 - b^2},$$

that combined with (14), yields:

$$\frac{t_m^2 c^2}{4} = \left(a\frac{ax}{a^2 - b^2} - x\right)^2 + b^2\sin^2\phi + h_s^2 \qquad (19)$$

$$= -\frac{b^2 x^2}{a^2 - b^2} + b^2 + h_s^2$$

$$= -\frac{b_e^2 x^2}{a_e^2 - b_e^2} + b_e^2,$$

where we have expressed the parameters of the ellipse on the ground as a function of the ellipsoid parameters by exploiting (8) and (9). We furthermore notice that $h^2 = a_e^2 - b_e^2$ and, from (16):

$$t_m^2 = \left(t_b^2 - \frac{4h^2}{c^2}\right)\left(1 - \frac{x^2}{h^2}\right)$$

$$= t_0^2\left(1 - \frac{x^2}{h^2}\right),$$

that is the smile, an ellipse in the (t_m, x) domain. The smile is the plot for $\psi = 0$ in Fig. 8.a.

3.5 The generalized smile in k-t coordinates

Using the same technique that we have used in [11], we can now move the generalized smile into the wavenumber time domain, simply by parameterizing the smile in terms of the time derivative

$$k_x = \frac{dt_m}{dx} = \frac{\partial t_m}{\partial\phi}\cdot\frac{\partial\phi}{\partial x}$$

rather than in terms of the abscissa x. The resulting function is again double valued and can be easily determined from the previous considerations. As an example, (18) and (19) have been exploited to compute the frequency domain expression of the delays:

$$t_m(k_x) = t_m(x(\phi)) + x(\phi) \cdot k_x(\phi)$$

represented in Fig. 8.b.

4 Motion compensation as bistatic focusing

As observed in the previous sections, we can also cover in the same way the case of motion compensation, i.e. the transfer of the data from one initial trajectory where they had been acquired, to any other, where they have to be focused. The geometry is shown in Fig. 9. The large circle on the ground underneath the sensor corresponds to the uniform distribution of scatterers that contribute to the initial survey with a single impulse at fast time t_0. Its radius is:

$$a = \sqrt{\left(\frac{ct_0}{2}\right)^2 - z_0^2}, \tag{20}$$

z_0 being the sensor height. We assumed that only an arc, marked as a thick line in the figure, is effectively illuminated by the antenna beam. The other two circles represents two uniform distributions of scatterers that contribute as two impulses in the second monostatic acquisition along the reference track. Their delays, to be compensated by the generalized smile, are proportional to the distances r_1 and r_2, in general: $r(x)$. The monostatic delay is then:

$$\frac{ct_m}{2} = \sqrt{z_1^2 + p(x)^2}, \tag{21}$$

where $p(x)$ is the horizontal projection of $r(x)$, and can be computed basing on the geometry of Fig. 10.a. The figure compares with Fig 7.b, now the single circular reflector centered on O, is to be replaced by the envelope of circles centered on the ground projection of the reference track, the line $y = d$. The distance $p(x)$ in (21) is either $|P' - C|$ or $|P - C|$, depending on the sign of y, i.e. the right/left looking of the sensor. We get:

$$p(x) = a \pm \sqrt{x^2 + d^2}$$

to be combined with (20) and (21) to derive the generalized "smile", plotted in Fig. 11. We notice that these kernels may have either the shape of a smile or of a frown. This second case comes from the arc corresponding to $y > d$, as Fig. 10.b shows.

As a conclusion of this short section, we have shown that motion compensation, i.e. to use the geophysical jargon, the continuation of the data from one sensor's trajectory to any other can be carried out by convolving with a generalized smile, as shown in Fig. 11. Notice that, also in the case of motion compensation, the parameters of the generalized smile require information about the DEM.

5 Conclusion

In this paper we have discussed bistatic SAR surveys focusing and the possibilities to transform a bistatic survey into the more usual monostatic one. We have shown how to extend and generalize the concept of smile (the transfer function between a bistatic and a monostatic survey) to non stationary acquisition geometries and to motion compensation; the structure of these generalized smiles shows the existence of cusps that indicate that for given illumination patterns and directions of flight such a reduction might be difficult. The cusps exist also in the constant offset case, but then they are limited to extreme squints and therefore not usually illuminated. However, in opportunity surveys, the geometry could be out of control, and therefore such situations may arise. We have also shown that a Digital Elevation Model is useful to focus bistatic data (but only if the offset is not constant and along the flight path) and in the case of motion compensation. The impact of the DEM imprecision, being it too dependent on the bistatic geometry and the resolution, is a priori unpredictable.

6 Acknowledgment

The authors would like to thank the anonymous reviewers who helped to improve this paper with a careful, complete, and detailed revision.

A Zero Doppler bistatic delay distance

In this appendix we compute the vertex of the DSR equation described by (5) in a very general case. The minimum of the DSR corresponds to the zero of f_τ, from (6):

$$\frac{\tau - \tau_{z1}}{\sqrt{(\tau - \tau_{z1})^2 + \tau_1^2}} = -\frac{1}{\sqrt{\mu\tau^2 + \tau_2^2}}\mu\tau \tag{22}$$

$$(\tau - \tau_{z1})\sqrt{\mu\tau^2 + \tau_2^2} = -\mu\tau\sqrt{(\tau - \tau_{z1})^2 + \tau_1^2}.$$

We square both terms, getting a 4^{th} order equation. Care should be taken as solutions of the squared equation are not necessarily solutions of (22):

$$\tau^4\left(\mu^2-\mu\right)-2\tau_{z1}\tau^3\left(\mu^2-\mu\right)+\tau^2\left(\left(\mu^2-\mu\right)\tau_{z1}^2-\tau_2^2+\mu^2\tau_1^2\right)+2\tau_{z1}\tau_2^2\tau-\tau_{z1}^2\tau_2^2=0.$$

Notice that the solution degenerates for the constant offset case: $\mu = 1$, however we do not care of this case, as there is already a closed form solution. We can make the replacements:

$$\begin{aligned} x &= \tau/\tau_{z1} \\ m &= \frac{\tau_2^2}{\left(\mu^2-\mu\right)\tau_{z1}^2} \\ k &= 1-\frac{\tau_2^2}{\left(\mu^2-\mu\right)\tau_{z1}^2}+\frac{\mu^2\tau_1^2}{\left(\mu^2-\mu\right)\tau_{z1}^2}, \end{aligned}$$

and the expression further simplifies as a function of two parameters:

$$x^4-2x^3+kx^2+2mx-m=0.$$

The solution is actually function of two parameters. We have a 4^{th} order equation with 4 solutions, of which two are real, and **only one is consistent** with (22). The solutions are:

$$x_1=\frac{1}{2}-\frac{1}{6}\sqrt{3}g+\frac{1}{6}\sqrt{3}\sqrt{\frac{6fg-4kfg-gf^2-gk^2+12\sqrt{3}fm+6\sqrt{3}fk-6\sqrt{3}f}{fg}}$$

$$x_2=\frac{1}{2}-\frac{1}{6}\sqrt{3}g-\frac{1}{6}\sqrt{3}\sqrt{\frac{6fg-4kfg-gf^2-gk^2+12\sqrt{3}fm+6\sqrt{3}fk-6\sqrt{3}f}{fg}}$$

where

$$p=\sqrt{81m^2k^2+162m^3k-162m^2k+3mk^4+81m^4-162m^3+3mk^3+81m^2-3mk}$$

$$f=\sqrt[3]{54mk+54m^2-54m+k^3+6p}$$

$$g=\sqrt{\frac{3f-2kf+f^2+k^2}{f}}.$$

References

[1] H D Griffiths. From a different perspective: principles, practice and potential of bistatic radar. In *CIE International Conference on Radar*, pages 1–7, 2003.

[2] Didier Massonnet. The interferometric cartwheel, a constellation of low cost receiving satellites to produce radar images that can be coherently combined. *International Journal of Remote Sensing*, 22(12):2413–2430, 2001.

[3] G Krieger, N Gebert, and A Moreira. Unambiguous SAR signal reconstruction from nonuniform displaced phase center sampling. *Geoscience and Remote Sensing Letters*, 1(4):260–264, July 2004.

[4] G Yates, A M Horne, A P Blake, R Middleton, and D B Andre. Bistatic SAR image formation. In *European Conference on Synthetic Aperture Radar, Ulm, Germany, 25–27 May 2004*, 2004.

[5] Huber Cantalloube, Michael Wendler, Vincent Giroux, Pascale Dubuois-Fernandez, and Gerhard Krieger. Challanges in SAR processing for airborne bistatic acquisitions. In *EUSAR'04, Ulm, Germany*, 2004.

[6] J H G Ender, I Walterscheid, and A R Brenner. New aspects of bistatic SAR: processing and experiments. In *International Geoscience and Remote Sensing Symposium, Anchorage, Alaska, 20–24 September 2004*, 2004.

[7] H G Ender. A step to bistatic SAR processing. In *European Conference on Synthetic Aperture Radar, Ulm, Germany, 25–27 May 2004*, 2004.

[8] L. Neo, F. H. Wong, and I. G. Cumming. Bistatic SAR processing using non-linear chirp scaling. In *Proceedings of the CEOS SAR Calibration Workshop*, 2004.

[9] Jesus Sanz-Marcos and Jordi J Mallorquí. A bistatic SAR simulator and processor. In *EUSAR'04, Ulm, Germany*, 2004.

[10] Mehrdad Soumekh. Wide bandwidth continuous wave monostatic/bistatic synthetic aperture radar imaging. In *International Conference on Image Processing, 4–7 October 1998*, volume 3, pages 361–365, 1998.

[11] Davide D'Aria, Andrea Monti Guarnieri, and Fabio Rocca. Focusing bistatic synthetic aperture radar using dip move out. *IEEE Transactions on Geoscience and Remote Sensing*, 42(7):1362–1376, 2004.

[12] Yu Ding and Jr David C Munson. A fast back-projection algorithm for bistatic SAR imaging. In *International Conference on Image Processing, Rochester, 22-25 October 2002*, volume 2, pages 441–444, 2002.

[13] O Loffeld, H Nies, V Peters, and S Knedlik. Models and useful relations for bistatic SAR processing. In *International Geoscience and Remote Sensing Symposium, Toulouse, France, 21–25 July 2003*, pages cdrom, 3 pages, 2003.

[14] S Deregowski and F Rocca. Geometrical optics and wave theory of constant offset sections in layered media. *Geophysical Prospecting*, 29:374–406, 1981.

[15] S Fomel. Theory of differential offset continuation. *Geophysics*, 68:718–732, 2003.

[16] J H G Ender and A R Brenner. PAMIR - a wideband phased array sar/mti system. *IEE Proceedings - Radar, Sonar, Navigation*, 150(3):165–172, 2003.

[17] G Bolondi, E Loinger, and F Rocca. Offset continuation of seismic sections. *Geophysical Prospecting*, 30:1045–1073, 1982.

[18] M Süss, B Grafmüller, and R Zahn. A novel, high resolution, wide swath SAR system. In *International Geoscience and Remote Sensing Symposium, Sydney, Australia, 9–13 July 2001*, pages 1013–1015, 2001.

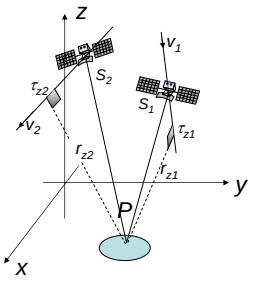

Figure 1: Generic bistatic geometry.

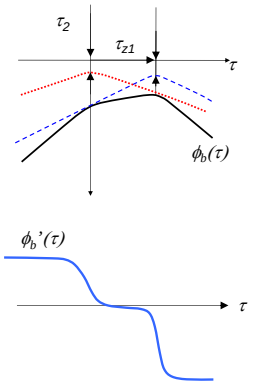

Figure 2: The Flat Top Hyperbola FTH. Up: The phase corresponds to the bistatic experiment, and thus is described by the Double Square Root expression correspondent to the sum of two monostatic terms. Down: the phase derivative.

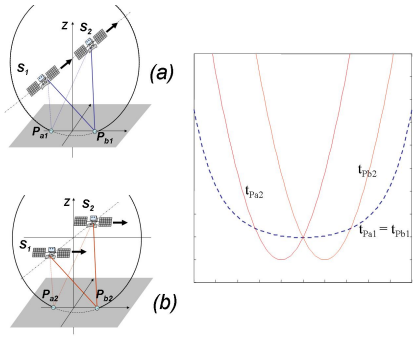

Figure 3: *Left*: Two targets, P_a and P_b in different locations are imaged by two bistatic systems where the sensors are: *(a)* aligned along the same orbit, or *(b)*: fly on parallel orbits. *Right:* In the first case focusing is actually 2D (DEM independent) as the same FTH results from both P_a and P_b. Not so in the second case.

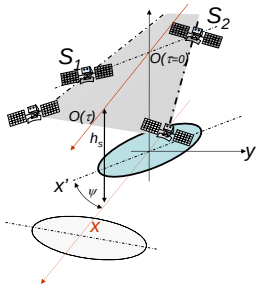

Figure 4: Geometry of the generalized bistatic acquisition: the sensors orbits are parallel to the ground.

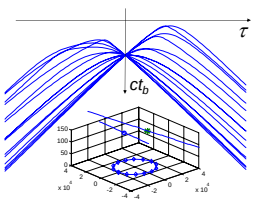

Figure 5: Using the push operator, we model back to the data space an elliptical distribution of scatterers (originally, a spike in the data space and thus an elliptical distribution of scatterers on a plane). For each scatterer in the model space belonging to the ellipse we associate a flat-top hyperbola in the data-space. The envelope of these hyperbolas reconstructs the spike. An extreme geometry (shown in the middle) has been assumed, to show the deformation of the FTH coming from different targets.

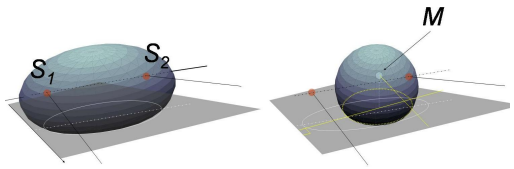

Figure 6: A spike in the data-space is the result of the illumination of the elliptic reflector on the left, intersection of the bistatic isochronal ellipsoid and the ground plane. This elliptic reflector can be modeled as a superposition of circles, each of them correspondent to a spike in the monostatic acquisition on the right. The radius of the sphere is proportional to the monostatic delay.

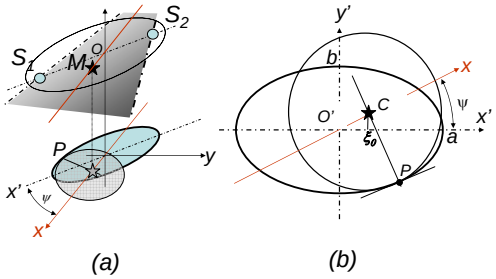

Figure 7: Geometry for the reduction of the bistatic survey to monostatic in the general case.

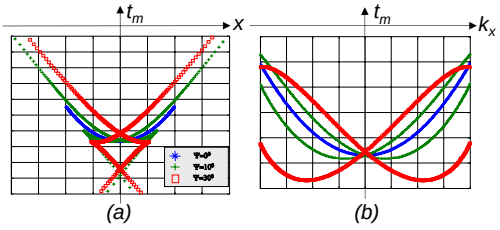

Figure 8: Plot of different generalized smiles, for different values of the ellipse rotation, ψ (a) in the (t, x) data domain, (b) in the (k_x, t) data domain.

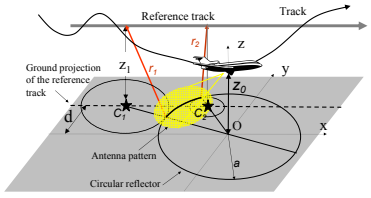

Figure 9: Geometry for the derivation of the motion compensation operator as a generalized smile.

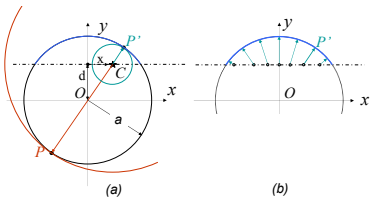

Figure 10: (a) Derivation of the motion compensation kernel, to be compared with Fig. 7. (b) The delays from the portion of the target $y > d$ decrease with $|x|$, generating a frown-like shape.

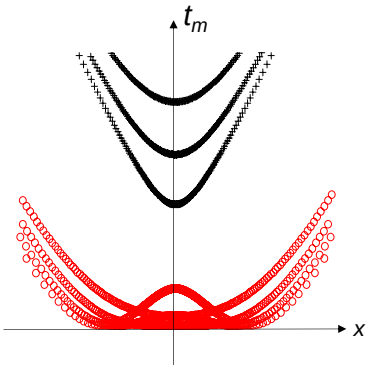

Figure 11: Smiles, upper plot (marked as '+'), and frowns, lower plots (marked as 'o') correspondent to the motion continuation case, for different distances with respect to the reference track, d.